

Effect of Grain Size on Hertzian Contact Damage in Alumina

Fernando Guiberteau,^{*†} Nitin P. Padture,^{*‡} and Brian R. Lawn^{*}

Materials Science and Engineering Laboratory, National Institute of Standards and Technology,
Gaithersburg, Maryland 20899

The role of microstructural scale on deformation–microfracture damage induced by contact with spheres is investigated in monophasic alumina ceramics over a range 3–48 μm in grain size. Measurement of a universal indentation stress–strain curve indicates a critical contact pressure ≈ 5 GPa, above which irreversible deformation occurs in alumina. A novel sectioning technique identifies the deformation elements as intragrain shear faults, predominantly crystallographic twins, within a confining subsurface zone of intense compression–shear stress. The twins concentrate the shear stresses at the grain boundaries and, above a threshold grain size, initiate tensile intergranular microcracks. Below this threshold size, classical Hertzian cone fractures initiate outside the contact circle. Above the threshold, the density and scale of subsurface-zone microcracks increase dramatically with increasing grain size, ultimately dominating the cone fractures. The damage process is stochastic, highlighting the microstructural discreteness of the initial deformation field; those grains which lie in the upper tail of the grain-size distribution and which have favorable crystallographic orientation relative to local shear stresses in the contact field are preferentially activated. Initial flaw state is not an important factor, because the contact process creates its own flaw population. These and other generic features of the damage process will be discussed in relation to microstructural design of polycrystalline ceramics.

I. Introduction

SURFACES of ceramic components in service are commonly subjected to concentrated loads, from contact bearings or spurious impacts with foreign bodies. The stresses from such contacts can introduce localized structural damage, which in turn can degrade the strength^{1,2} or erode the surface.³ Depending on the contact geometry, individual cracks may initiate from preexisting flaws or from precursor “plastic” deformation.^{4,5} In polycrystalline ceramics, the nature of the fracture damage can be controlled by events at the microstructural level. There is then a need to focus on the “short-crack” aspects of fracture. This need has been foreshadowed in toughness-curve (T -curve, or R -curve) studies on alumina and other ceramics that exhibit grain-interlock bridging.^{6–15} Thus, whereas increasing the grain size of alumina enhances the long-crack toughness, it simultaneously diminishes the strength¹⁶ and wear resistance.¹⁷ Grain

size might therefore be expected to play a vital role in determining the nature and degree of contact damage.

In a recent paper,¹⁸ the nature of contact-induced damage in a “coarse” (grain size 23 μm) alumina was studied using the Hertzian test. The Hertzian geometry, in which a spherical indenter is used to deliver concentrated stresses over a small area of specimen surface, usefully simulates “blunt” in-service contact conditions.⁴ In addition, because the contact pressure increases monotonically with applied load, the geometry allows one to trace the “indentation stress–strain” response of a material, from initial elastic contact through first irreversible deformation to a final “fully plastic” state.¹⁹ In that earlier study on alumina,¹⁸ damage was found to initiate in the subsurface region of high compression–shear *beneath* the contact instead of in the surface region of weak tension *outside* the contact. Intragrain shear–fault deformation, specifically crystallographic twinning and slip in the alumina, was identified as the primary stage of damage. Grain boundary microcracking at the ends of the constrained shear faults was identified as the secondary stage. Repeat contacts revealed severe mechanical fatigue;¹⁸ in severe cases grain boundary microcracks coalesced into a fragmentation zone, resulting in the detachment of grains from the surface. Some comparative experiments on a “fine” alumina (grain size 2.5 μm) showed no detectable microcracking, suggesting that microstructural scale plays a critical role in the contact damage process.

In this paper we examine more systematically the role of grain size on contact damage from single-cycle Hertzian contacts in polycrystalline alumina. We find that above a contact pressure ≈ 5 GPa, independent of grain size or sphere size, the contact deviates from an ideal Hertzian elastic response, indicating the onset of “plasticity.” We also examine more closely the nature of the subsurface deformation–microcrack damage, using a novel sectioning technique, and monitor the damage rate during the load–unload cycle, using acoustic emission. Our experiments indicate that twin/slip shear faults within individual grains do indeed play a controlling precursor role in the initiation of grain-boundary microcracks, that the bulk of the microcrack initiation occurs during the latter part of the *loading* half-cycle, and that the damage process has a strong stochastic element in the polycrystalline structure. The experiments also indicate the existence of a threshold grain size ≈ 20 μm for initiation; on traversing this threshold, the microcrack density increases with grain size. Finally, we consider some of the broader implications of our observations on alumina in relation to microstructural design of structural ceramics for contact-related applications.

II. Experimental Procedure

Polycrystalline aluminas with mean grain sizes 3, 9, 15, 21, 35, and 48 μm were obtained from an earlier study on toughness curves.¹⁶ The processing of those aluminas was carried out in a class A-100 clean room to minimize impurity content. The resulting microstructures were fully dense and uniform, with a narrow size distribution of equiaxed grains⁸ and small flaw population. In contrast, the commercial material used in our earlier

M. V. Swain—contributing editor

Manuscript No. 194390. Received July 14, 1993; approved September 30, 1993.

Supported by the U.S. Office of Naval Research. Special financial support was received for F. Guiberteau from the Ministerio de Educación y Ciencia (DGICYT), Spain.

^{*}Member, American Ceramic Society.

[†]Guest Scientist from Departamento de Física, Universidad de Extremadura, 06071, Badajoz, Spain.

[‡]Guest Scientist from Department of Materials Science and Engineering, Lehigh University, Bethlehem, PA 18015.

⁸In accordance with the “Hillert criterion” (maximum diameter < twice mean diameter).

Hertzian contact fatigue experiments¹⁸ had a much wider grain size distribution and a higher population of pores, inclusions, and grain boundary triple-point flaws.

Bar specimens 20 mm × 2.5 mm × 2.5 mm of each grain size alumina were diamond polished to 1- μm grade finish. Some specimens were used for indentation stress–strain measurements. The polished surfaces of these specimens were coated with gold prior to indentation. Normal indentations were made in a universal testing machine (Model 1122, Instron, Canton, MA) at constant crosshead speed (1.67 $\mu\text{m}\cdot\text{s}^{-1}$) over a load range $P = 0$ to 2000 N, using tungsten carbide spheres of radii $r = 1.98, 3.18, 4.76, 7.94,$ and 12.7 mm, in air. The contact radius a for each indentation was measured from residual impressions left in the gold coating, to enable evaluations of contact pressure ($p_0 = P/\pi a^2$) and indentation strain (a/r) (see Sect. III(1)). In the inelastic region, the contact radius always exceeded the maximum grain size by at least an order of magnitude.

Subsurface indentation damage could be seen below the contacts of uncoated specimens in dark-field illumination, especially in the coarser aluminas.¹⁸ In the present study an alternative, more revealing observational technique was developed, following a precontact section procedure originally used by Mulhearn²⁰ and others,²¹ as follows:

(i) Polished surfaces of two specimens were bonded face-to-face under clamping pressure with a thin layer (<10 μm) of adhesive (Loctite, Newington, CT).

(ii) A surface perpendicular to the bonded interface was ground and polished along the length of the specimen.

(iii) The newly polished surface was indented symmetrically across the surface trace of the interface (Fig. 1). Since the principal stresses directly beneath the contact area are highly compressive,⁴ the opposite surfaces in the region of subsurface damage are constrained from moving apart, precluding potential artifacts associated with free surface effects.²²

(iv) The two halves of the indented bar were separated by dissolving the glue in acetone, cleaned, gold-coated, and viewed using Nomarski interference illumination.

With this procedure, shear fault features not evident in conventional polished sections were readily visible in the Nomarski contrast as shallow surface offsets on the separated free surfaces.

Acoustic emission experiments were performed to quantify the sequence of damage evolution during indentation. Acoustic

activity was recorded during the load–unload indentation cycle using a piezoelectric transducer attached to the specimen indentation surface with rubber cement (LOCAN 320, Physical Acoustics, Princeton, NJ). Data were recorded as accumulated signal energy vs elapsed time at constant crosshead displacement speed.

Some dummy indentation stress–strain tests were made on a tungsten carbide plate cut from one of the larger spheres, to examine the limiting contact conditions for purely reversible deformation of the indenting spheres.

III. Results

(1) Indentation Stress–Strain Curve

The Hertzian test can be used to obtain an indentation stress–strain curve^{19,23} for deformable solids which would otherwise, in more uniformly tensile loading geometries, behave in a perfectly brittle manner. Measurements of contact radius a , sphere radius r , and indentation load P (Fig. 1) enable one to evaluate

$$\text{Indentation stress } p_0 = P/\pi a^2 \quad (1a)$$

$$\text{Indentation strain } a/r \quad (1b)$$

Indentation stress–strain functions $p_0(a/r)$ have been previously measured for lithium fluoride,²³ silicate glasses,²⁴ and zinc sulfide;²¹ more recently, curves have been obtained for a commercial alumina (grain size 23 μm)¹⁸ and a glass–ceramic.²⁵

Indentation stress–strain data for the *finest* and *coarsest* of the aluminas investigated in the present study (grain sizes 3 and 48 μm) are plotted in Fig. 2. The results for the two grain sizes are indistinguishable within the experimental scatter. Also included as the solid curve in Fig. 2 is an empirical data fit from our earlier study on a commercial alumina with *intermediate* grain size.¹⁸ The dashed lines represent asymptotic limits for the indentation stress–strain curve: the lower inclined dashed line is the linear relation for purely elastic contacts from Hertzian theory²³

$$p_0 = (3E/4\pi k)(a/r) \quad (\text{elastic}) \quad (2)$$

where $E = 393$ GPa is Young's modulus of the alumina and $k = 0.88$ for tungsten carbide on alumina,^{18,26,27} the upper horizontal dashed line is an indentation hardness $H = 19.0 \pm 2.0$ GPa, common to all grain sizes, obtained from Vickers tests.¹⁶

The overlap in data in Fig. 2 suggests the existence of a “universal” stress–strain curve for alumina, implying a critical stress condition for deformation independent of grain size or preexisting flaw state. The data deviate below the Hertzian line at pressures above $p_0 \approx 5$ GPa, marking the onset of “yield.” Independent stress–strain tests using tungsten carbide spheres on plates of the same material show deviations above ≈ 6 GPa, indicating that part of the deviation at the higher stress end of the curve in Fig. 2 could be due to deformation of the sphere.

(2) Optical Microscopy

Optical microscopy confirms that the above-mentioned deviation from Hertzian behavior in Fig. 2 (sphere deformation notwithstanding) is due to the onset of indentation damage in the alumina. The nature of this damage can be deduced from the micrograph sequences in Figs. 3 and 4, obtained using the bonded-interface section technique described in Sect. II. Figure 3 shows how the subsurface damage develops in the coarsest (48 μm) alumina as one proceeds up the stress–strain curve in Fig. 2. Thus, the sequence A–B–C–D shows section views at increasing indentation pressure. The initiation of the deformation–microfracture subsurface damage zone, and subsequent expansion of this zone, are immediately apparent from the free-surface relief displacements revealed by the Nomarski contrast. At $p_0 = 5.3$ GPa in A, i.e., just above the elastic limit in Fig. 2, just 3 to 4 grains have deformed. At increased pressures, $p_0 = 6.2$ GPa in B and 7.0 GPa in C, the number of

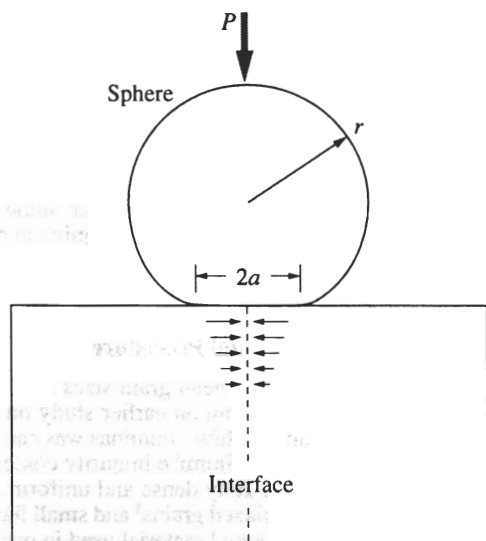


Fig. 1. Hertzian test geometry, for bonded-interface specimen. Sphere radius r delivers load P over contact radius a . Specimen consists of two polished halves glued together across interface. Compressive stresses beneath contact (arrows) maintain contact between specimen halves during indentation.

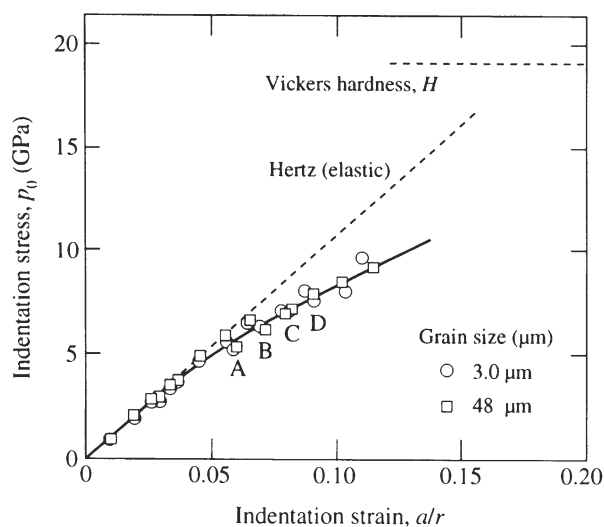


Fig. 2. Indentation stress-strain curve. Data are for aluminas of 3- and 48- μm grain size. Inclined dashed line is Hertzian elastic response, and upper horizontal dashed line is hardness (averaged over all grain sizes). A, B, C, and D correspond to micrographs in Fig. 3. Solid curve is an empirical fit to the data for a commercial alumina (grain size 23 μm) from a previous study.¹⁸

deformed grains increases, and the damage zone expands toward the surface. At $p_0 = 8.0$ GPa in D, the damage is more profuse and begins to take on the appearance of the well-developed, near-hemispherical deformation zone expected from continuum plasticity models.¹⁹

The presence of shear faults traversing the width of some of the deformed grains is clearly evident as deformation (presumably twin) lamellae in the micrographs. Microcracks extending along those grain boundaries intersected by the lamellae are also evident, by virtue of greatly enhanced interference contrast from attendant surface-grain displacements and rotations. At the higher pressures these microcracks tend to link up with neighbors. The microcracks appear to be associated *only* with deformed grains, suggesting that the shear faults are a necessary precursor to fracture damage in these materials. We note also the variability in orientation of the lamellae, indicating strong crystallographic features in the damage pattern.

The set of micrographs in Fig. 4 shows both half-surface (upper) and section views (lower) of indentations for each of the aluminas, at indentation pressure $p_0 = 8.0$ GPa. Again, the damage is confined within a relatively well-defined hemispherical deformation zone below the contact circle. Note that the section views reveal the subsurface damage more clearly than the half-surface views, reinforcing the utility of the bonded-interface sectioning technique. The apparent universality of the stress-strain curve for the two grain sizes in the indentation stress-strain curve of Fig. 2 (together with the common Vickers hardness value for all grain sizes) suggests that the net plastic

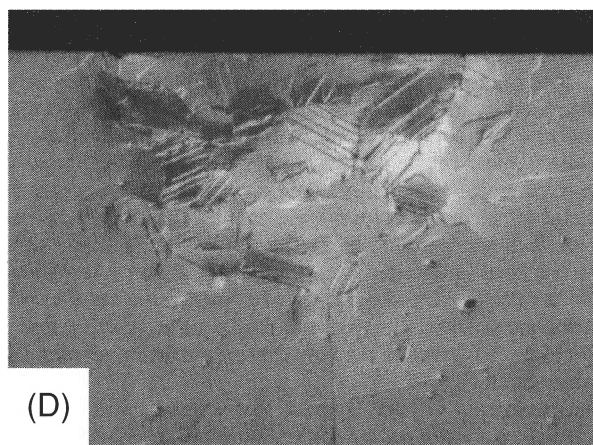
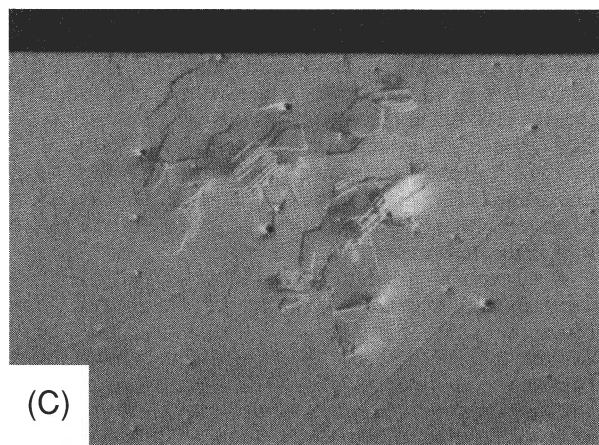
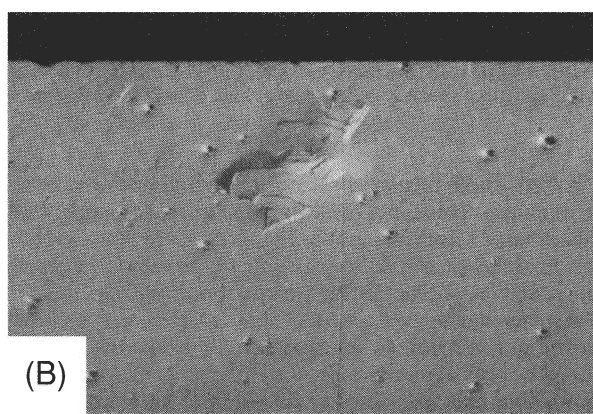
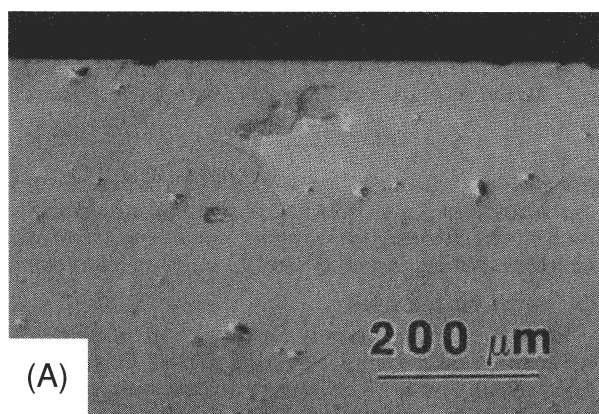


Fig. 3. Optical micrographs in Nomarski illumination showing section views of indentation sites in alumina of grain size 48 μm . Indentations made with WC ball of radius $r = 3.18$ mm, at increasing contact pressures p_0 : (A) 5.3, (B) 6.2, (C) 7.0, and (D) 8.0 GPa (cf. points A–D in Fig. 2).

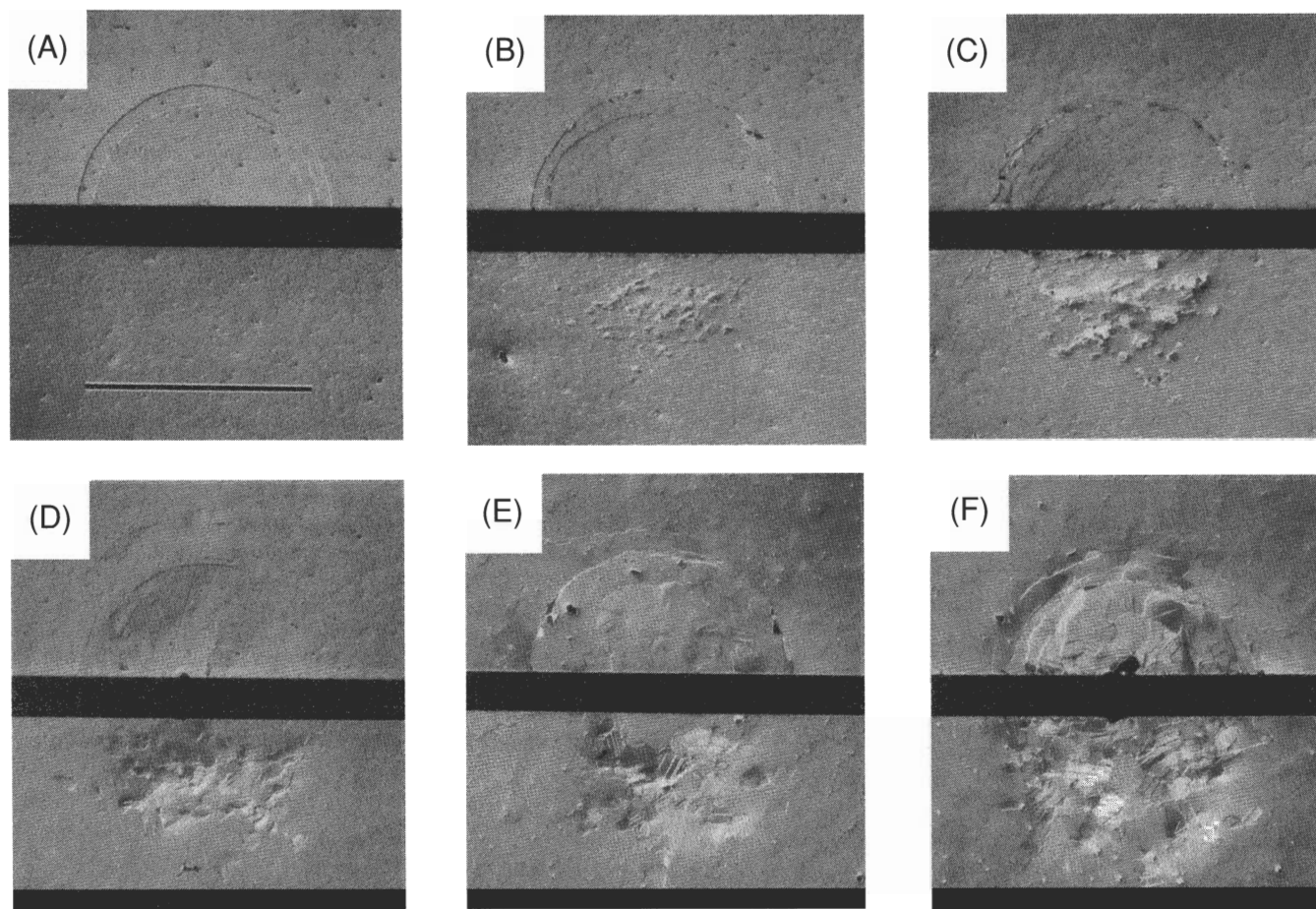


Fig. 4. Optical micrographs in Nomarski illumination showing half-surface (top) and section (bottom) views of indentation sites in aluminas with grain size (A) 3 μm , (B) 9 μm , (C) 15 μm , (D) 21 μm , (E) 35 μm , and (F) 48 μm . Indentations made at a fixed indentation pressure $p_0 = 8.0$ GPa, using WC sphere of radius $r = 3.18$ mm at load $P = 2000$ N (cf. point D in Fig. 2). Marker in (A) represents contact diameter $2a = 550$ μm .

deformation within this subsurface zone should be the same for all the aluminas. This is not clear from the micrographs. Indeed, with the finest (3 μm) material in Fig. 4(A) there is no obvious indication of any plastic deformation at all; however, the reduction in attendant microcracking inevitably diminishes the surface displacements, and thence the interference contrast. Moreover, at this level we are approaching the limits of spatial resolution of optical microscopy.

Again, confined, shear-fault-initiated microfracture damage *beneath* the contact circle is clearly evident in the coarsest (48 μm) material (Fig. 4(F)), but appears to diminish progressively with decreasing grain size in Fig. 4. There are indications of a threshold in the crack initiation process. This trend to diminished microfracture damage with diminishing grain size is accompanied by an increasing tendency to macrocrack formation *outside* the contact circle; in the finest (3 μm) material (Fig. 4(A)), the fracture pattern closely resembles the classical Hertzian cone crack in ideally homogeneous solids.⁴ Cone fracture is inhibited in the coarser materials by the larger scale of crack deflections, particularly in the subsurface Hertzian field where enforced deflection from the principal stress trajectory surface results in a rapid build-up of compressive stresses.^{28,29} Thus, for the coarsest alumina, the partial cone crack at lower right in Fig. 4(F) arrests at the very first subsurface grain boundary intersection.

Another feature in Figs. 3 and 4 that warrants special comment is the stochastic nature of the deformation–microfracture damage pattern. It is clear that not all grains in the active deformation zone participate in the damage process. The shear faults in those grains that do deform show wide variability in planar

orientation within the Hertzian field. Note further that the damage patterns in Figs. 3(D) and 4(F) differ considerably from each other, although the loading conditions were identical. Grain orientation, as well as size, is clearly an important factor.

(3) Acoustic Emission

Plots of cumulative acoustic energy versus elapsed time during load–unload indentation cycles for the six aluminas for a fixed sphere size ($r = 3.18$ mm) are shown in the upper diagram of Fig. 5. The corresponding indentation pressure (at constant crosshead displacement rate), to a maximum value $p_0 = 8$ GPa, is included in the lower diagram.

From the plots in Fig. 5 it is evident that all six aluminas show acoustic activity. There is an initial inactivity as the pressure builds up and ultimately exceeds the elastic limit. We note that the bulk of the activity occurs toward the end of the loading half-cycle, as the system traverses the upper reaches of the data in Fig. 2. Relatively minor activity is observed during the unloading half-cycle. There is a clear discreteness in the acoustic traces, indicating the existence of well-defined local instabilities in the deformation–fracture process.

A systematic trend to increased activity is apparent with increasing grain size. Fewer, but larger, discrete jumps are observed in the finer aluminas (3, 9, and 15 μm) during the loading half-cycle. These jumps correlate with the pop-in of Hertzian cone cracks (Figs. 4(A–C)). More frequent, but smaller, jumps are observed in the coarser aluminas (21, 35, and 48 μm). The bulk of the activity in these latter cases appears to correlate with progressive initiation of the subsurface microfracture damage (Figs. 3(A–D)), although the underlying source of the emissions (e.g., crack pop-in) is not unequivocally

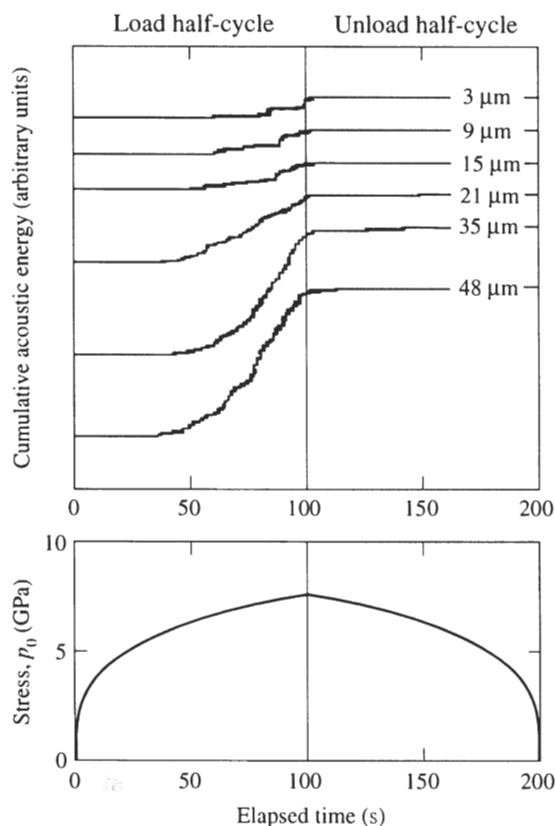


Fig. 5. Plots of cumulative acoustic energy (arbitrary linear scale) versus elapsed time during single load-unload indentation cycle at constant crosshead speed in alumina specimens (upper diagram), using WC sphere of radius $r = 3.18$ mm. Variation of contact pressure with time indicated (lower diagram).

identified in our tests. Note also that the onset of acoustic activity occurs earlier in the load cycle with increasing grain size. To show the scaling trend more clearly, we plot in Fig. 6 the cumulative energy over the full load-unload cycle as a function of grain size. There is a distinctive, although not abrupt, transition in the integrated signal at grain size ≈ 20 μm. These results suggest the existence of a grain-size threshold (vertical dashed line in Fig. 6) above which copious new sources of acoustic emission are activated.

IV. Discussion

In this paper we have used Hertzian indentation to investigate the deformation and microfracture in polycrystalline aluminas over a range of grain sizes. Our results reveal departures from an ideally brittle response, as measured on a nonlinear indentation stress-strain curve. Such departures are associated with the generation of a deformation-microfracture damage zone, here revealed by a novel sectioning technique, in the confined region of strong compression and shear stresses *beneath* the indenter.¹⁸ The fully developed damage zone is made up of an accumulation of microstructurally discrete events, each consisting of some kind of intragrain shear faulting accompanied by intergrain microcracking. This cumulative damage zone is quite different from the continuous Hertzian cone fracture that occurs in the weak tensile region *outside* the contact circle in classically homogeneous brittle materials.^{4,5,28} The alumina microstructure imposes itself strongly on the contact damage pattern.

The issue of primary interest here in relation to this departure from classical Hertzian cone fracture toward cumulative subsurface microcracking is the effect of grain size. Recall the dramatic enhancement of this transition with progressive microstructural coarsening in Fig. 4. Now, size effects are not

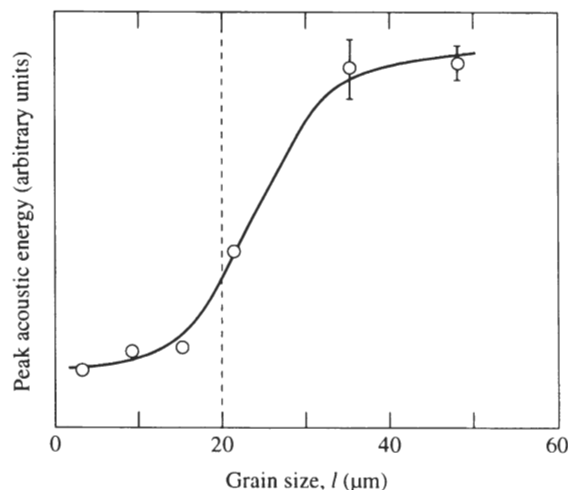


Fig. 6. Plot of peak acoustic energy (i.e., cumulative energy at end of load-unload cycle) as a function of grain size, for data obtained using ball of radius $r = 3.18$ mm, at peak contact pressure $p_0 = 8.0$ GPa (cf. Fig. 5).

uncommon in brittle cracks where some kind of competition between deformation (volume-controlled) and fracture (area-controlled) is involved.^{5,30-32} This is true even of Hertzian tests in *homogeneous* solids (e.g., glasses and single crystals), where the use of ever-smaller spheres suppresses cone fracture in favor of subsurface shear-fault deformation, reflecting the well-documented transition in indentation response from "blunt" to "sharp."^{4,5,24} In Fig. 4, however, the indenter radius is held fixed, so we are dealing here exclusively with microstructural scaling.

It is therefore of interest to consider the nature of the deformation-microfracture pattern more closely in this context of microstructural scaling.

(1) Deformation

The existence of a universal nonlinear stress-strain curve in Fig. 2 for alumina, *independent* of grain size, reflects an intrinsic "plasticity" in the mechanical response at high contact pressures. The curve deviates from the Hertzian elastic prediction above $p_0 \approx 5$ GPa, corresponding to an "indentation yield stress" for the material.^{19,23} This deviation, together with the observation in Fig. 3 that the damage initiates *beneath* the contact in the region of maximum shear, implies that the deformation component is governed by some critical faulting stress.¹⁸ The micrographs in Figs. 3 and 4 show the subsurface faults in the alumina to be in the form of twin/slip bands contained within individual grains, arrested at their ends by the grain boundaries. The characteristic scale of individual faults within each grain is therefore governed by the grain size. On the other hand, the apparent universality of the curve and hardness values for the aluminas in Fig. 2 indicates that the *net* deformation is not limited by the grain size, i.e., that the integrated volume of deformed material over the contact zone is microstructurally invariant.

Positive identification and detailed analysis of the fundamental microshear processes responsible for the contact deformation in the aluminas, particularly at the finer grain sizes, are issues for further study.

(2) Microfracture

On the other hand, grain size has a strong effect on the microcracking damage. This is reflected most dramatically in the acoustic emission data in Fig. 5. Close inspection of the micrographs in Figs. 3 and 4 indicates that the microcracks initiate from the lamella shear faults and extend over one to three grain facets. The lack of any acoustic activity during *unloading* suggests that microcrack *pop-in* occurs only during the loading half-cycle. However, such microcracks will be subject to

intense constraining hydrostatic compression at full load, so a significant proportion of the extension may actually take place *stably* (and *quietly*) on *release* of the compression during unloading (cf. growth of lateral cracks during unloading in sharp-indenter fields.^{4,33}) The amount of extension from each microcrack nucleus will depend critically on the sign and intensity of residual thermal expansion anisotropy stresses at the grain boundary; clearly, the greatest extension will occur from those facets that experience tensile stresses. These same stresses will also limit the extension of the microcracks, as they encounter compressive facets and become increasingly subject to grain-bridging tractions.¹²

This deformation–microfracture description allows us to construct a simplistic model for the influence of grain size on contact-induced microfracture in alumina. Consider a volume element in the compression–shear deformation zone beneath the contact circle, as shown in the schematic of Fig. 7. Here, $-\sigma_1$ and $-\sigma_3$ are principal compression stresses in the Hertzian field. Those compression stresses are generally unequal, so there is a component of shear acting on planes inclined to the principal axes, attaining a maximum value $\frac{1}{2}(\sigma_1 - \sigma_3)$ at 45° . The shear component initiates intragrain faults FF, which arrest at the weak grain boundaries and generate stress intensities there. If the stress intensities exceed a critical level, microcracks FC pop in. A critical condition for such pop-in may be determined by regarding the faults FF as shear cracks with net shear tractions $S = |\tau| - \mu|\sigma| - \tau_F$ at their interfaces.^{34,35} τ and σ are resolved shear and (compressive) normal components of the contact stress field at the fault plane, directly proportional to the mean contact pressure p_0 ; μ is a coefficient of sliding friction between contacting surfaces; and τ_F is an intrinsic fault cohesion (e.g., twinning) stress. A minimum requirement for crack initiation is that the yield point on the indentation stress–strain curve in Fig. 2 should be exceeded, corresponding to $S = S_Y$, with S_Y a material constant. Then one may write a stress-intensity factor $K = \psi S_Y l^{1/2}$ for the shear fault, with l a grain dimension and ψ a crack geometry term dependent on the angle between FF and FC.⁵ Microcrack initiation occurs along FC when the stress intensity equals the grain boundary toughness, i.e., $K = T_0$, corresponding to a critical grain size

$$l_c = (T_0/\psi S_Y)^{1/2} \quad (3)$$

A more comprehensive analysis of microcrack initiation, including a description of the subsequent propagation into the adjacent microstructure, will be given elsewhere.³⁶

Two aspects of the deformation–microfracture observations reported in Sect. III that warrant special consideration are *stochastics* and *flaw sensitivity*. The stochastic nature of the microstructurally discrete damage alluded to in Sect. III(2) appears to be the result of a complex interplay of statistical variation in both relative size and crystallographic orientation of individual grains. Even the most uniform polycrystals, including the aluminas used in the present study, are characterized by a distribution of grain sizes about a mean; and twin/slip deformation of alumina occurs only on certain preferred crystallographic planes.³⁷ Hence the largest, “correctly” oriented grains in the Hertzian compression–shear zone will deform first, resulting in a grain-by-grain activation within the ultimate deformation zone as one progresses up the indentation stress–strain curve. This stochastic element will inevitably reflect in Eq. (3), accounting for the lack of an abrupt grain size cutoff (vertical dashed line) in Fig. 6.

Flaw sensitivity is of interest in relation to the susceptibility of polycrystalline ceramics to damage accumulation in contact stress fields. Of particular interest is the issue of preexisting (e.g., processing) flaws vs contact-induced flaws. In Fig. 2, stress–strain data from the present study obtained on equiaxed, homogeneous, “defect-free” aluminas¹⁶ overlap (at least within experimental scatter) the solid curve from a previous study on a nonequiaxed, inhomogeneous, commercial alumina with a relatively high density of large processing flaws.¹⁸ This implies that preexisting defect populations are not of great consequence to contact damage of the kind observed in Figs. 3 and 4. The contact process generates its own flaw population, via the precursor shear faulting.

These results have important implications concerning the microstructural design of ceramics for improved contact-damage resistance. Most obvious is the refinement of grain size, to minimize the prospect of microcrack initiation. Such an approach is not inconsistent with precedent work on the wear of ceramics, where decreased grain size leads to demonstrably reduced removal rates.^{17,38–40} However, the insensitivity of contact damage to preexisting flaws suggests processing strategies quite different from the traditional ones in which preexisting flaw populations are painstakingly eliminated.⁴¹ Instead, the emphasis shifts to refining the grain-size distribution, to avoid the occasional large grain or grain cluster. Again, we would emphasize that some of these strategies may run counter to those required for improved long-crack toughness, especially in ceramics that exhibit toughening by grain-interlock bridging.^{6–15}

Another interesting materials design aspect pertains to the effect of environment-assisted slow-crack growth, particularly from atmospheric water, on contact damage.¹⁸ Since the contact deformation initiates in the *subsurface* Hertzian field, the ensuing microcracks do not have access to the external chemical environment, at least not until the damage zone becomes sufficiently large that it intersects the contact surface. This suggests that the effect of slow-crack growth may play no role in the early developmental stages of the deformation–microfracture process. Under such conditions the observation of damage *accumulation* in *repeated* contacts¹⁸ can be attributed to a true mechanical fatigue process.

Although we have focused our attention here exclusively on alumina, the basic features of the Hertzian deformation–microfracture damage process envisaged in Fig. 7 may be considered generic to heterogeneous ceramics. Key to this kind of damage is the existence of weak planes in the microstructure, either intragrain or intergrain, so that some kind of easy shear faulting may occur in the subsurface compression–shear zone. In the case of alumina, the faulting is in the form of crystallographic lamellae within individual grains. Intersection of the lamellae

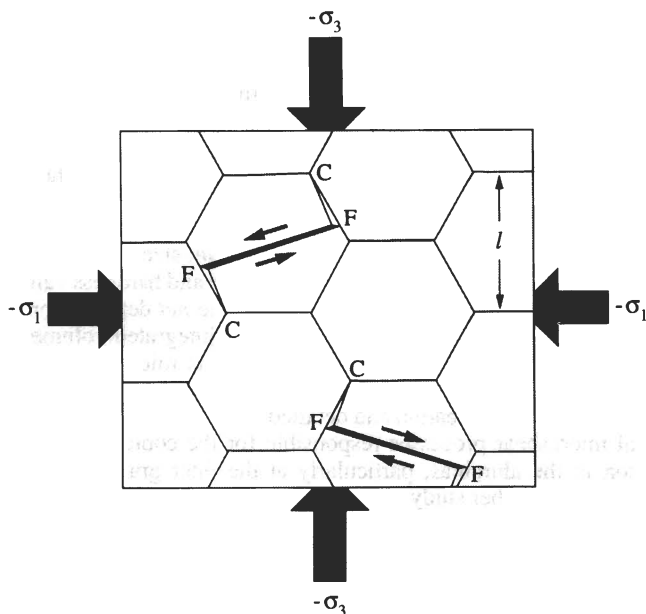


Fig. 7. Schematic of deformation–microfracture damage in polycrystalline alumina ceramic, grain size l . Volume element is subjected to compressive normal stresses $-\sigma_1$ and $-\sigma_3$ along contact axis below spherical indenter. Shear stresses (arrows) initiate intragrain lamellae FF, which pop-in intergrain microcracks FC at their ends.

with the weak grain boundaries allows for a concentration of stress intensity, which in turn facilitates intergranular microcracking. Other faulting mechanisms are identified in other ceramic types: in softer monophase polycrystals, e.g., magnesium oxide, straightforward crystallographic slip;⁴² in silicate glasses, a breakdown of the network structure at the theoretical cohesive shear stress;⁴³⁻⁴⁶ in machinable glass-ceramics, sliding at weak interfaces between crystallized mica flakes and the glass matrix;²⁵ in complex rocks, a multiplicity of intrinsic and extrinsic frictional sliding defect planes.³⁴ This suggests that, while fine details of the slip process may be material-specific, the larger concept of deformation-induced damage in Hertzian contact fields is broadly applicable.

It is therefore evident that the Hertzian test offers certain benefits as a means for investigating the general deformation and fracture properties of brittle ceramics. Some of this information, in particular that relating to the deformation component, is not accessible using conventional strength and toughness tests, because in those tests the inevitable dominance of tensile stresses promotes the propagation of a single well-developed crack at the expense of potentially competitive shear processes. To obtain information on such shear processes it is necessary to contrive a test procedure with a high component of hydrostatic compression to suppress or restrict the fracture, as in the traditional (but complex) confined-pressure apparatus used by geophysicists.³⁴ Vickers (or Knoop) hardness indentation is the one routine form of mechanical testing used by ceramists that does provide the necessary high shear component for activation of irreversible deformation. The relative advantage of the Hertzian test is that one can study the evolution of the damage pattern, from initial elastic to final fully plastic contact, providing information on the short-crack microfracture processes that control fundamental fatigue and wear properties of brittle ceramics.

Acknowledgments: We thank H. Cai and M. A. Stevens Kalceff for fruitful discussions and S. J. Bennison and P. Chantikul for providing the alumina specimens.

References

- ¹S. M. Wiederhorn and B. R. Lawn, "Strength Degradation of Glass Resulting from Impact with Spheres," *J. Am. Ceram. Soc.*, **60** [9-10] 451-58 (1977).
- ²B. R. Lawn and D. B. Marshall, "Indentation Fracture and Strength Degradation in Ceramics"; pp. 205-29 in *Fracture Mechanics of Ceramics*, Vol. 3. Edited by R. C. Bradt, D. P. H. Hasselman, and F. F. Lange. Plenum, New York, 1978.
- ³S. M. Wiederhorn and B. J. Hockey, "Effect of Material Parameters on the Erosion Resistance of Brittle Materials," *J. Mater. Sci.*, **18** [3] 766-80 (1983).
- ⁴B. R. Lawn and T. R. Wilshaw, "Indentation Fracture: Principles and Applications," *J. Mater. Sci.*, **10** [6] 1049-81 (1975).
- ⁵B. R. Lawn, *Fracture of Brittle Solids*. Cambridge University Press, Cambridge, U.K., 1993.
- ⁶R. Knehan and R. Steinbrech, "Effect of Grain Size on the Resistance Curves of Al_2O_3 ," *Sci. Ceram.*, **12**, 613-19 (1983).
- ⁷F. Deuerler, R. Knehan, and R. Steinbrech, "Testing Methods and Crack Resistance Behaviour of Al_2O_3 ," *Sci. Ceram.*, **13**, C-617-C-621 (1986).
- ⁸M. V. Swain, "R-Curve Behaviour in a Polycrystalline Alumina Material," *J. Mater. Sci. Lett.*, **5**, 1313-15 (1986).
- ⁹P. L. Swanson, C. J. Fairbanks, B. R. Lawn, Y.-W. Mai, and B. J. Hockey, "Crack-Interface Grain Bridging as a Fracture Resistance Mechanism in Ceramics: I. Experimental Study on Alumina," *J. Am. Ceram. Soc.*, **70** [4] 279-89 (1987).
- ¹⁰P. L. Swanson, "Crack-Interface Traction: A Fracture-Resistance Mechanism in Brittle Polycrystals"; pp. 135-55 in *Advances in Ceramics*, Vol. 22, *Fractography of Glasses and Ceramics*. Edited by J. Varner and V. D. Frechette. American Ceramic Society, Columbus, OH, 1988.
- ¹¹R. W. Steinbrech and O. Schmenkel, "Crack Resistance Curves of Surface Cracks in Alumina," *J. Am. Ceram. Soc.*, **71** [5] C-271-C-273 (1988).
- ¹²S. J. Bennison and B. R. Lawn, "Role of Interfacial Grain-Bridging Sliding Friction in the Crack-Resistance and Strength Properties of Nontransforming Ceramics," *Acta Metall.*, **37** [10] 2659-71 (1989).

- ¹³G. Vekinis, M. F. Ashby, and P. W. R. Beaumont, "R-Curve Behaviour of Al_2O_3 Ceramics," *Acta Metall.*, **38** [6] 1151-62 (1990).
- ¹⁴N. Ramachandran and D. K. Shetty, "Rising Crack-Growth-Resistance (R-Curve) Behavior of Toughened Alumina and Silicon Nitride," *J. Am. Ceram. Soc.*, **74** [10] 2634-41 (1991).
- ¹⁵L. M. Braun, S. J. Bennison, and B. R. Lawn, "Objective Evaluation of Short-Crack Toughness Curves Using Indentation Flaws: Case Study on Alumina-Based Ceramics," *J. Am. Ceram. Soc.*, **75** [11] 3049-57 (1992).
- ¹⁶P. Chantikul, S. J. Bennison, and B. R. Lawn, "Role of Grain Size in the Strength and R-Curve Properties of Alumina," *J. Am. Ceram. Soc.*, **73** [8] 2419-27 (1990).
- ¹⁷S.-J. Cho, B. J. Hockey, B. R. Lawn, and S. J. Bennison, "Grain-Size and R-Curve Effects in the Abrasive Wear of Alumina," *J. Am. Ceram. Soc.*, **72** [7] 1249-52 (1989).
- ¹⁸F. Guiberteau, N. P. Padture, H. Cai, and B. R. Lawn, "Indentation Fatigue: A Simple Cyclic Hertzian Test for Measuring Damage Accumulation in Polycrystalline Ceramics," *Philos. Mag. A*, **68** [5] 1003-16 (1993).
- ¹⁹D. Tabor, *Hardness of Metals*. Clarendon, Oxford, U.K., 1951.
- ²⁰T. O. Mulhearn, "The Deformation of Metals by Vickers-Type Pyramidal Indenters," *J. Mech. Phys. Solids*, **7**, 85-96 (1959).
- ²¹S. v. d. Zwagg, J. T. Hagan, and J. E. Field, "Studies of Contact Damage in Polycrystalline Zinc Sulphide," *J. Mater. Sci.*, **15**, 2965-72 (1980).
- ²²N. P. Padture, "Postfailure Subsidiary Cracking from Indentation Flaws," *J. Mater. Res.*, **8** [6] 1411-17 (1993).
- ²³M. V. Swain and B. R. Lawn, "A Study of Dislocation Arrays at Spherical Indentations in LiF as a Function of Indentation Stress and Strain," *Phys. Status Solidi*, **35** [2] 909-23 (1969).
- ²⁴M. V. Swain and J. T. Hagan, "Indentation Plasticity and the Ensuing Fracture of Glass," *J. Phys. D: Appl. Phys.*, **9**, 2201-14 (1976).
- ²⁵H. Cai, M. A. Stevens Kalceff, and B. R. Lawn, "Deformation and Fracture of Mica-Containing Glass-Ceramics in Hertzian Contacts," *J. Mater. Res.*, **9** [3] 762-70 (1994).
- ²⁶H. Hertz, *Hertz's Miscellaneous Papers*; Ch. 5 and 6. Macmillan, London, U.K., 1896.
- ²⁷K. L. Johnson, *Contact Mechanics*. Cambridge University Press, London, U.K., 1985.
- ²⁸F. C. Frank and B. R. Lawn, "On the Theory of Hertzian Fracture," *Proc. R. Soc. London, A*, **299** [1458] 291-306 (1967).
- ²⁹B. R. Lawn, "Hertzian Fracture in Single Crystals with the Diamond Structure," *J. Appl. Phys.*, **39** [10] 4828-36 (1968).
- ³⁰B. R. Lawn and D. B. Marshall, "Hardness, Toughness, and Brittleness: An Indentation Analysis," *J. Am. Ceram. Soc.*, **62** [7-8] 347-50 (1979).
- ³¹K. E. Puttick, "Energy Scaling, Size Effects and Ductile-Brittle Transitions in Fracture," *J. Phys. D: Appl. Phys.*, **12**, L19-L23 (1979).
- ³²K. Puttick, "The Correlation of Fracture Transitions," *J. Phys. D: Appl. Phys.*, **13**, 2249-62 (1980).
- ³³B. R. Lawn and M. V. Swain, "Microfracture beneath Point Indentations in Brittle Solids," *J. Mater. Sci.*, **10** [1] 113-22 (1975).
- ³⁴J. C. Jaeger and N. G. W. Cook, *Fundamentals of Rock Mechanics*. Chapman and Hall, London, U.K., 1971.
- ³⁵H. Horii and S. Nemat-Nasser, "Compression-Induced Microcrack Growth in Brittle Solids: Axial Splitting and Shear Failure," *J. Geophys. Res.*, **90** [B4] 3105-25 (1985).
- ³⁶B. R. Lawn, N. P. Padture, F. Guiberteau, and H. Cai, "A Model for Microcrack Initiation and Propagation beneath Hertzian Contacts in Polycrystalline Ceramics," *Acta Metall. Mater.*, in press (1994).
- ³⁷M. L. Kronberg, "Plastic Deformation of Single Crystals of Sapphire," *Acta Metall.*, **5** [9] 507-24 (1957).
- ³⁸C. C. Wu, R. W. Rice, D. Johnson, and B. A. Platt, "Grain-Size Dependence of Wear in Ceramics," *Ceram. Eng. Sci. Proc.*, **6** [7-8] 995-1011 (1985).
- ³⁹R. W. Rice, "Micromechanisms of Microstructural Aspects of Ceramics Wear," *Ceram. Eng. Sci. Proc.*, **6** [7-8] 940-58 (1985).
- ⁴⁰S.-J. Cho, H. Moon, B. J. Hockey, and S. M. Hsu, "The Transition from Mild to Severe Wear in Alumina during Sliding," *Acta Metall.*, **40** [1] 185-92 (1992).
- ⁴¹F. F. Lange, "Powder Processing Science and Technology for Increased Reliability," *J. Am. Ceram. Soc.*, **72** [1] 3-15 (1989).
- ⁴²T. L. Johnston, R. J. Stokes, and C. H. Li, "Crack Nucleation in Magnesium Oxide Bicrystals under Compression," *Philos. Mag.*, **7**, 23-34 (1962).
- ⁴³J. T. Hagan and M. V. Swain, "The Origin of Median and Lateral Cracks at Plastic Indents in Brittle Materials," *J. Phys. D: Appl. Phys.*, **11** [15] 2091-102 (1978).
- ⁴⁴A. Arora, D. B. Marshall, B. R. Lawn, and M. V. Swain, "Indentation Deformation/Fracture of Normal and Anomalous Glasses," *J. Non-Cryst. Solids*, **31** [3] 415-28 (1979).
- ⁴⁵J. T. Hagan, "Shear Deformation under Pyramidal Indenters in Soda-Lime Glass," *J. Mater. Sci.*, **15**, 1417-24 (1980).
- ⁴⁶B. R. Lawn, T. P. Dabbs, and C. J. Fairbanks, "Kinetics of Shear-Activated Indentation Crack Initiation in Soda-Lime Glass," *J. Mater. Sci.*, **18** [9] 2785-97 (1983). □